Analytical modelling of Tm-doped tellurite glass including cross-relaxation process.

Ali Albalawi [a,*] Charlie Brilliant[a] Alessandro Chiasera[b] Hrvoje Gebavi[c] Rolindes Balda[d] Maurizio Ferrari[b] Wilfried Blanc[e] Wedad Albalawi[f] Hazel Hung[a] Alexander Quandt[g] Anna Lukowiak[h] and Stefano Taccheo[a]

[a] Laser and Photonics Group, College of Engineering, Swansea University, Bay Campus, Swansea, UK
[b] Istituto di Fotonica e Nanotecnologie - CNR, Povo (Tn), Italia.
[c] Department of Materials physics, Ruđer Bošković Institute Bijenička cesta 54, 10000 Zagreb.
[d] Applied Physic Department I, University of the Basque Country, UPV-EHU, Bilbao and Materials Physics Center CSIC-UPV/EHU, San Sebastian, Spain
[e] Institut de Physique de Nice, Université Côte d'Azur, CNRS UMR7010, Parc Valrose, 06108 Nice Cedex 2, France.
[f] Princess Nourah bint Abdulrahman University, Mathematics Department, College of Science, PO Box 84428, Riyadh, KSA.
[g] University of the Witwatersrand, Physics Building, 2050 Johannesburg, South Africa
[h] Institute of Low Temperature and Structure Research PAS, Wroclaw, Poland

ARTICLEINFO

Article history:
Received ……
Received in revised form
……
Accepted ……..

Keywords:
Thulium laser
Reverse cross relaxation
Energy transfer

ABSTRACT

In this paper, we present a comprehensive analytical model of Tm able to take into account direct cross-relaxation process. We show that by using an appropriate set of parameters the model is able to properly fit the first part of the fluorescence decay of Tm-doped tellurite glasses for different dopant concentration values. We also compare the model with a full numerical model to investigate its limitations. We assess the model is a valid tool to fit fluorescence properties but for predicting population inversion is limited to doping level up to about 1%. In case of higher doping the reverse cross-relaxation process becomes significant,.
.

1. Introduction

Thulium's (Tm^{3+}) wide emission spectrum plays a vital role in numerous infrared laser applications, including precision cutting, the surgical removal of body tissues, and sensing [1-5]. Furthermore, Tm^{3+} is characterized by the cross-relaxation process ($^3H_4$, $^3H_6 \rightarrow {}^3F_4$, $^3F_4$), which involves the promotion of two ions into the laser's upper level with a single pump photon, making it a very efficient laser system. Although the consequence of this cross-relaxation process is the enhancement of pumping quantum efficiency, along with lasing at 1.8 µm, almost all laser simulations neglect to take into consideration, or alternatively, neglect to take direct measurements of the reverse cross-relaxation process ($^3F_4$,$^3F_4 \rightarrow {}^3H_6$,$^3H_4$), which is noteworthy since it reduces the efficacy of cross-relaxation process [6, 7].

Several glass host materials have been use, among them we include tellurite, silica, germanate, and fluoride glasses [8-12]. Tellurite glasses, amongst of all the oxide glasses, have lower photon energies (approximately 750 cm^{-1}), and they also provide high rare earth ion solubility. Independently from the type of glass, the design process which underpins the development of lasers depends on precision modeling, along with the comparative examination of various doping levels [13, 14]. Despite the abundant evidences relating to lifetimes and cross-sections, the parameters associated with ion-ion interactions (i.e., cross-relaxation and the reverse transfer process) [6, 13-17] are more difficult to obtain or cannot be identified in a straightforward manner. For this reason in previous paper we carefully study a set of Tm-doped glass samples [15] with doping level ranging from 0.36 mol% to 10% mol (corresponding to doping levels ranging from 0.82 to $22*10^{20}$ ion/cm^{-3}) [6], and calculate the direct [6] and, recently, the reverse cross-relaxation parameters [18] with the results of being able to fit the whole set of samples and to show the impact on pumping efficiency [18]. While numerical modelling is a powerful approach, analytic modelling may lead to better understanding of the system and allow for find for example, intensity noise suppression guidelines allowing effective circuit design or modelling of chaotic behaviour, as done for Er-doped systems [19, 20]. For this reason in this paper, we present a new analytical model able for the first time, to the best of our knowledge, to consider the direct cross relaxation process. To evaluate the validity of this model we compare it with a set of experimental data and a full numerical model, including the reverse cross-relaxation process [18]. We show that our analytical model is able to fit the first part of the fluorescence decay signal but, as expected, fails when the reverse cross-relaxation process becomes important. We quantify the discrepancy with comparison with the full numerical model we assess the analytic approach is a valid tool in case of limited doping level.

2. Theoretical modelling

The energy levels scheme and the transitions used in the model are depicted in Fig. 1 [14, 21].

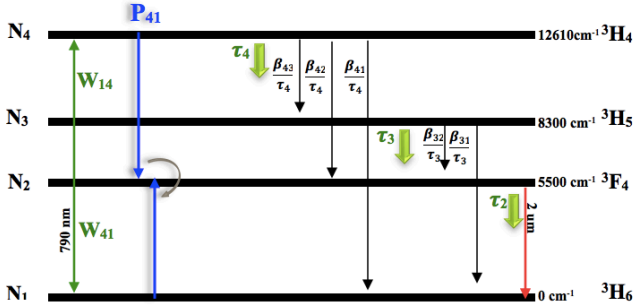

Fig. 1: Energy level scheme and transitions of thulium considered for the analytical model

Fig.1 shows the lowest four energy manifolds of the Tm^{3+} ion. In the figure, the laser transition, the pump transition, and direct and reverse cross relaxation processes are indicated, together with spontaneous decay paths. The corresponding set of rate equations is:

$$\frac{dN_4}{dt} = W_{14}N_1 - W_{41}N_4 - \frac{N_4}{\tau_4} - P_{41}N_4N_1 \quad (1)$$

$$\frac{dN_3}{dt} = -\frac{N_3}{\tau_3} + \frac{\beta_{43}N_4}{\tau_4} \quad (2)$$

$$\frac{dN_2}{dt} = 2P_{41}N_4N_1 - \frac{N_2}{\tau_2} + \frac{\beta_{42}N_4}{\tau_4} + \frac{\beta_{32}N_3}{\tau_3} \quad (3)$$

$$\frac{dN_1}{dt} = W_{14}N_1 + W_{41}N_4 - P_{14}N_4N_1 + \frac{N_2}{\tau_2} + \frac{\beta_{41}N_4}{\tau_4} + \frac{\beta_{31}N_3}{\tau_4} \quad (4)$$

where N_1 ,N_2 ,N_3 and N_4 are the population of the energy levels $^3H_6$ (ground level), $^3F_4$ (upper laser level), $^3H_5$ and $^3H_4$ (pump level), respectively; W_{14} ,W_{41} , are the pump rates, τ_i is the lifetime of the i-level, and β_{ij} are branch ratios from the i- to j-level [15]. The coefficients P_{ij} describe the energy transfer processes: P_{41} ($^3H_4$, $^3H_6 \rightarrow {}^3F_4$, $^3F_4$) is the cross relaxation constant, which is proportional to doping level [15] The above set of equation

is similar to the one used in Ref. [18], without the reverse cross-relaxation phenomenon ($^3F_4,^3F_4 \rightarrow ^3H_6,^3H_4$) taken into account, we will assess its impact in section 4.

Through solving the rate equations at steady state, we calculate the population values for each level mathematically as follow:

In eq. (1) we set $A_4 = \frac{1}{\tau_4}, A_3 = \frac{1}{\tau_3}, A_{43} = \frac{\beta_{43}}{\tau_4}, A_{42} = \frac{\beta_{42}}{\tau_4}$, and $A_{32} = \frac{\beta_{32}}{\tau_3}$

We rewrite eq.1 as

$$-N_4(W_{41} + A_4 + P_{41}N_1) + W_{14}N_1 = 0$$

This gives

$$N_4 = \frac{W_{14}N_1}{W_{41}+A_4+P_{41}N_1} \quad (5)$$

From eq. (2) we then get

$$N_3 = \frac{hW_{14}N_1}{W_{41}+A_4+P_{41}N_1} \quad (6)$$

where $h = \frac{A_{43}}{A_3}$

From Eq. 3

$$2P_{41}N_4N_1 - A_2N_2 + A_{42}N_4 + A_{32}N_3 = 0$$

We obtain

$$N_2 = \frac{2P_{41}N_4N_1+A_{42}N_4+A_{32}N_3}{A_2} \quad (7)$$

and by substituting N_4 and N_3 from eq. (5) and (6) into eq. (7) we obtain.

$$N_2 = \left(\frac{2P_{41}N_1}{A_2} * \frac{W_{14}N_1}{W_{41}+A_4+P_{41}N_1}\right) + \left(\frac{A_{42}}{A_2} * \frac{W_{14}N_1}{W_{41}+A_4+P_{41}N_1}\right) + \left(\frac{A_{32}}{A_2} * \frac{hW_{14}N_1}{W_{41}+A_4+P_{41}N_1}\right) \quad (8)$$

If we now use the constant total ion condition.

$$N_{tot} = N_1 + N_2 + N_3 + N_4 \quad (9)$$

We get

$$N_{tot} = N_1 + \left(\frac{2P_{41}N_1}{A_2} * \frac{W_{14}N_1}{W_{41}+A_4+P_{41}N_1}\right) + \left(\frac{A_{42}}{A_2} * \frac{W_{14}N_1}{W_{41}+A_4+P_{41}N_1}\right) + \left(\frac{A_{32}}{A_2} * \frac{hW_{14}N_1}{W_{41}+A_4+P_{41}N_1}\right) + \frac{hW_{14}N_1}{W_{41}+A_4+P_{41}N_1} + \frac{W_{14}N_1}{W_{41}+A_4+P_{41}N_1} \quad (10)$$

To simplify the expression we now define the following coeffients.

$$b = \frac{2P_{41}W_{14}}{A_2} \text{ and } c = \frac{A_{42}W_{14}}{A_2} \text{ and } r = \frac{A_{32}hW_{14}}{A_2}$$

And we rewrite Eq. 10 as

$$N_{tot}(W_{41} + A_4 + P_{41}N_1) = N_1(W_{41} + A_4 + P_{41}N_1) + bN_1^2 + cN_1 + rN_1 + hW_{14}N_1 + W_{14}N_1 \quad (11)$$

If we now make N_1 the subject of Eq.10 we obtain a quadratic expression which solution is:

$$N_1 = \frac{+B-\sqrt{B^2+4*A*C}}{-2A} \quad (12)$$

Where A, B and C are

$$C = N_{tot}W_{41} + N_{tot}A_4$$
$$B = (-N_{tot}P_{41} + W_{41} + A_4 + c + r + hW_{14} + W_{14})$$
$$A = P_{41} + b$$

We note the chose one out of the two possible mathematical solutions since a Physical problem has only one solution, the other mathematical solutions has no Physical meaning.

3. Simulation and comparison with experimental data

To test the analytical model we fit the fluoresce decay curves of a set of Tellurite glass samples. The experimental data were reported in details in Ref. [15, 18]. Numerical values use in the simulations are listed in Table 1 for the four samples presented, with a doping level ranging from 0.36 mol% to 7 mol%. The pump cross section at 790 nm is taken from Ref [15] while the emission cross-section is calculated using Ref [22]. To simulate the pumping condition with non-instantaneous pump power decay, the pump intensity was set to $1.3*10^3$ W/cm^2, assuring a low excitation regime, and pump power decreasing is simulated by using an exponential decay curve with a 2 μs time constant [18].

Table 1: List of parameters

Parameters	symbols	values		Ref.
Coefficient of Cross Relaxation	Cr	$1.81*10^{-23}$ m^3 s^{-1} mol^{-1}		[6]
Pump wavelength	λ_p	790 nm		
Cross Relaxation	P_{41}	Mole of sample*Cr(m^3 s^{-1})		[6]
Coefficient of Reverse Cross Relaxation	a	0.03		[18]
Absorption pump	σ_{ap}	$8*10^{-25}$ m^2		[15]
Emission pump cross	σ_{ep}	$2.2*10^{-25}$ m^2		[22] *
Pump Intensity	I_p	$1.3*10^3$ W/cm^2		
Branch ratio	β_{41}	$^3H_6 \rightarrow ^3H_4$	0.9038	[15]
	β_{42}	$^3H_4 \rightarrow ^3F_4$	0.0762	[15]
	β_{43}	$^3H_4 \rightarrow ^3H_5$	0.02	[15]
	β_{31}	$^3H_5 \rightarrow ^3H_6$	0.9793	[15]
	β_{32}	$^3H_5 \rightarrow ^3F_4$	0.0207	[15]
Lifetime	0.36 mol%wet	τ_2	$2.9*10^{-3}$	[18]
		τ_4	$443*10^{-6}$	[18]
	1.08 mol%wet	τ_2	$2.35*10^{-3}$	[18]
		τ_4	$245*10^{-6}$	[18]
	4 mol%wet	τ_2	$0.43*10^{-3}$	[18]
		τ_4	$8.2*10^{-6}$	[18]
	7 mol%wet	τ_2	$0.16*10^{-3}$	[18]
		τ_4	$6*10^{-6}$	[18]

* Calculated by McCumber equation from [22]

Fig. 2 (left) shows the experimental data fitting using the analytical program for the four samples with doping level 0.36 mol%, 1.08 mol%, 4mol% and 7mol%. On Fig 2 (Right) is reported the same fitting using the full numerical model that consider reverse cross-relaxation[18]. We notice that we have an excellent fitting in the first part of the decay curve thus proving the validity of our approach and his suitability for spectroscopy and dynamic investigation [19]. However in Ref [18] we recently point out the impact of reverse cross-relaxation on the second part of the decay curve, with a longer time constant related to the reverse cross-relaxation process [6, 13-16, 23]. We demonstrated that when the $^3H_4$ population is almost depleted, and almost all ions are back to ground state, a second exponential constant kick in experimentally, and this may effect pumping efficiency [18]. The evaluation of the discrepancy between the analytic model and a full numerical model, including reverse cross-relaxation process, is therefore important to assess the range of validity of our new analytical model when level populations have to be predicted.. This is discussed in the next section

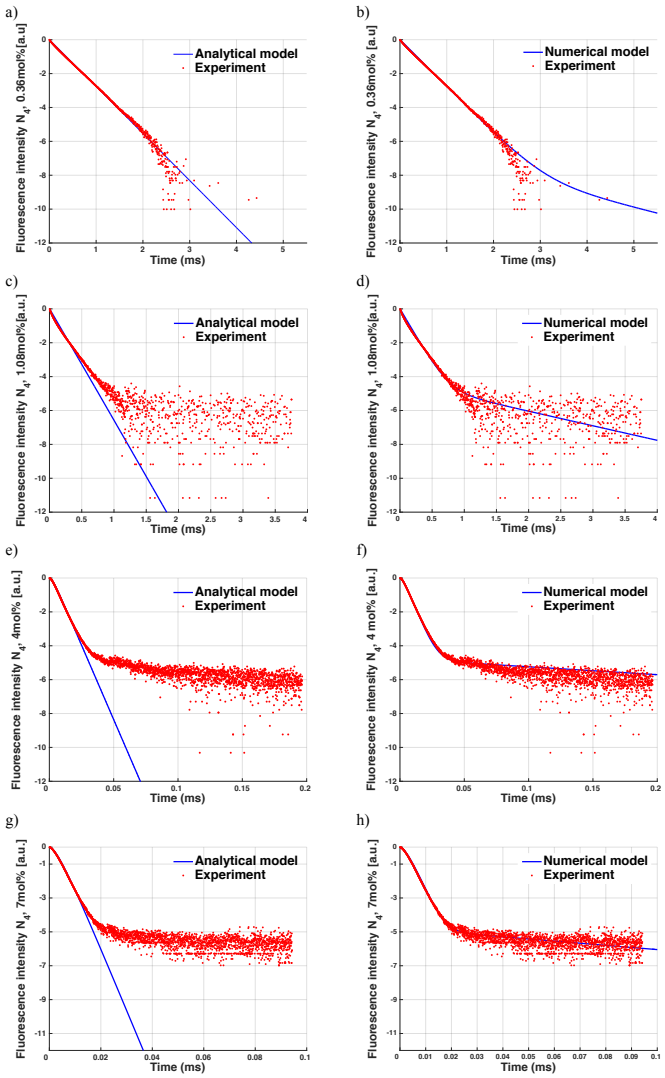

Fig. 2: Experimental data and comparison with analytical simulation (left) and with numerical simulation (right) [18]

4. Comparison analytical and numerical simulation

This section assesses the discrepancy with the full model, which includes the reverse cross-relaxation process. While this process was so far manly neglected, especially due to not available specific spectroscopic data, in Ref [18] we show that it could be one of the reason while Tm-lasers exhibits lower then expected efficiency [34]. For this purpose this paragraph deal with the error generated in calculating the population of main levels by neglecting the reverse cross relaxation phenomenon.

Fig. 3 compares the four energy level population values normalized to the total number of ions, N_i/N_t being Nt the doping level of the specific sample.

Fig. 4 shows instead of the same horizontal scale the normalised laser inversion $(N_2-N_1)/N_t$.

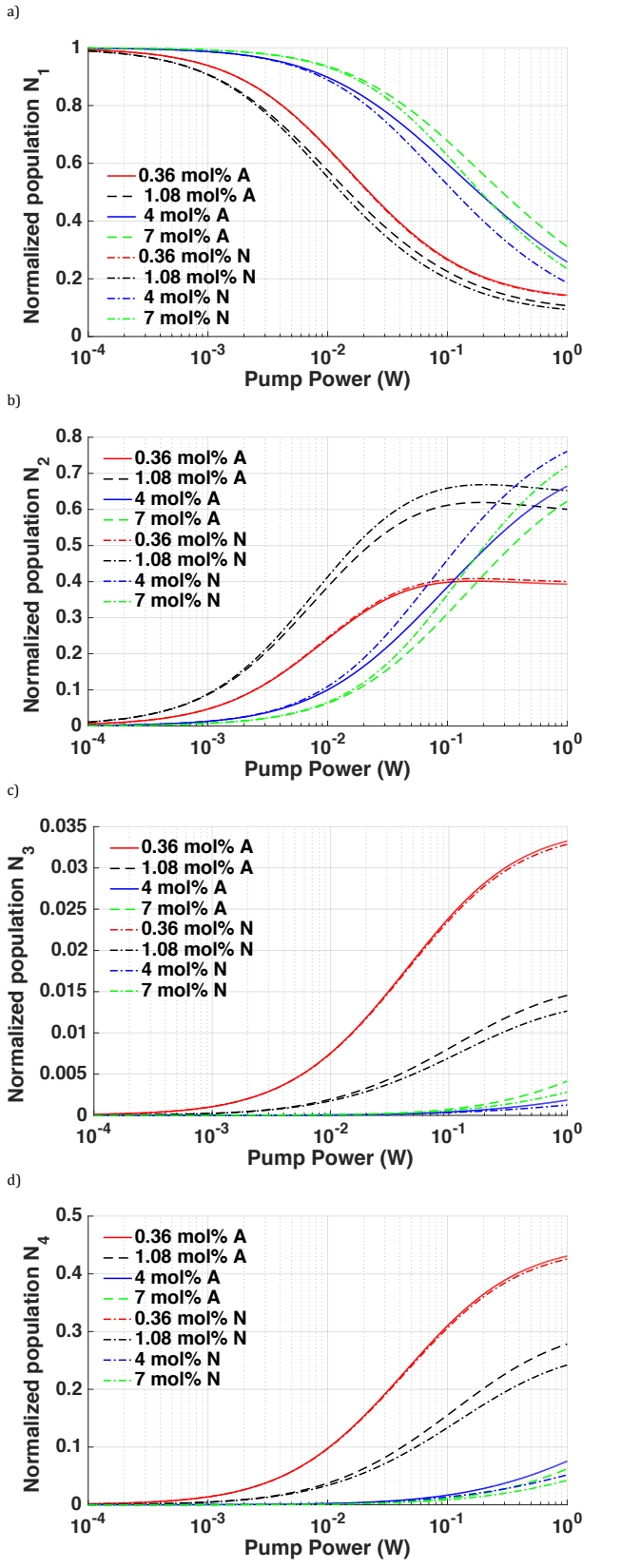

Fig. 3: Normalised population of N_1,N_2,N_3 and N_4 levels for the four samples using both numerical (N) (solid lines) and analytical (A) (dot-dashed and dashed lines)

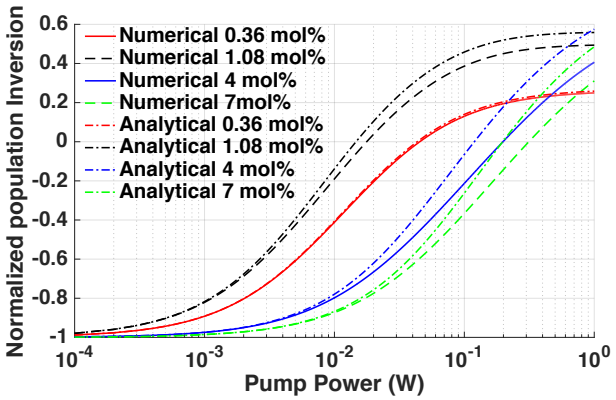

Fig. 4: Normalised Population Inversion calculated with numerical model (solid lines) and analytical model (dot-dashed and dashed lines)

Fig. 3 and Fig. 4 shows a negligible difference between our model and the numerical one when low pump power is considered and therefore the inversion level is low, which is the common situation for spectroscopic and fluorescence measurements. However the discrepancy becomes noticeable as the pump power increases and for samples with higher concentration samples. In particular since the error in the calculation of N_1 and N_2 has opposite sign, a significant difference arises in case of larger doping level and high pump power when population inversion, key laser design parameter, is considered as shown in Fig. 4. his also indicates the systems which may suffer larger errors could be power amplifier devices where high inversion to suppress spontaneous emission is required. We notice that, as expected, as overall features the analytical model always overestimate N_2 population and therefore the expected inversion.

To better appreciate the difference in Fig. 5 we shows the error ratio for N_1, N_2 and N_4 population, as defined as:

$$\text{Error ratio} = \frac{N_A - N_N}{N_N}$$

where N_A is population calculated by the analytical simulation and N_N is population calculated using the full numerical model. Note that in this case the normalization is with respect the numerical value and not the doping level.

(a)

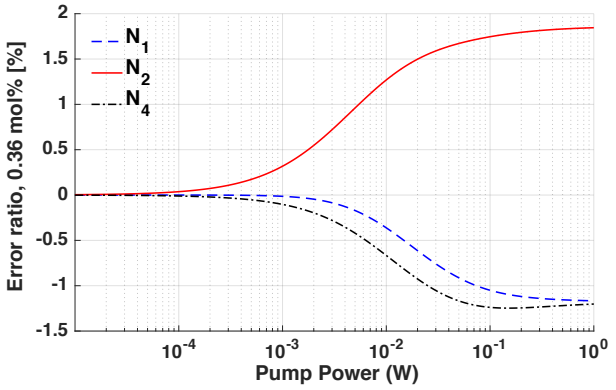

(b)

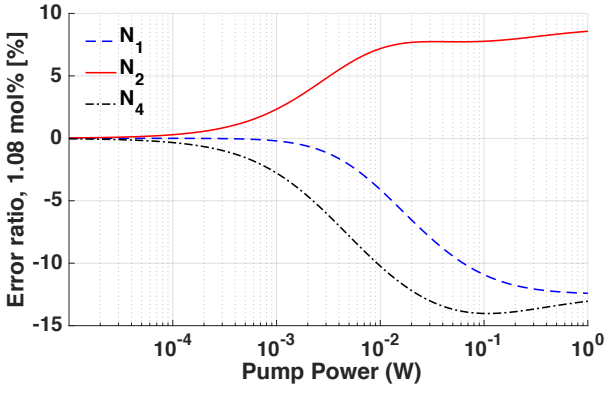

(c)

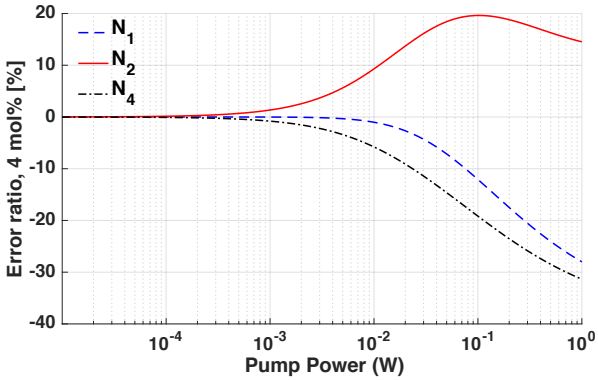

(d)

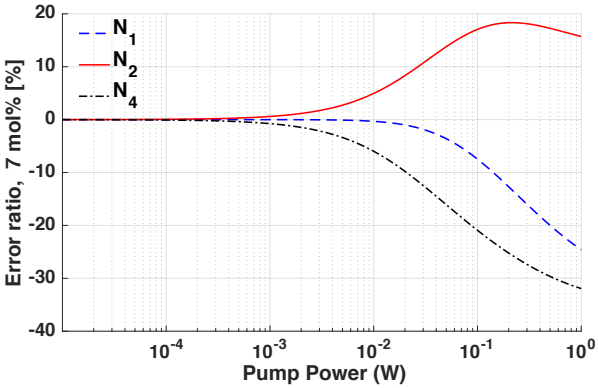

Fig. 5: Error ratio for each sample resulting of neglecting reverse cross relaxation

Fig. 5 confirms that for doping level up to about 1% the difference is within about 10%-15%. Fig. 6 shows instead the normalized population inversion difference, $[(N_2\text{-}N_1)_A\text{-}(N_2\text{-}N_1)_N]/N_t$, between the two approaches. Again we see that above 1 mol% doping level the difference may become significant and the analytic model, as any model neglecting the reverse cross-relaxation process [18] may fail.

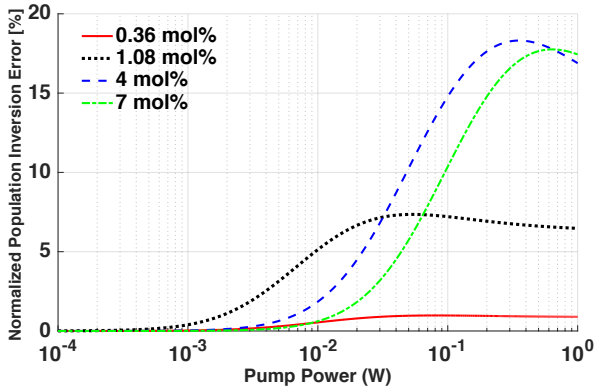

Fig. 6: Normalized Population Inversion Error

5. Impact on device operation

In Ref [18] we defined the impact of reverse cross relaxation process by introducing parameter *a*, and calculated the required pump intensity to reach a given value of inversion for each parameter *a* which were equal 0, 0.01, 0.03 and 0.084. By the above definitions *a*=0 refers to the case of no reverse cross-relaxation, i.e. the analytical model, case *a*=0.03 to the set of tellurite glass samples we investigated [18] and *a*= 0.084 to silica host [13]

Fig. 7 shows, for a sample with 1.08 mol% doping level, the pump intensity required to reach a given inversion. Values have been normalized to the value at *a*= 0; The values chose for *a* are 0.01 to simulate a low reverse cross relaxation parameter Fig. 7 therefore shows the discrepancy in the calculated laser intensity required to achieved a stated inversion. The reason this discrepancy is larger then the one on laser inversion (see Fig.6) is because the well know non-linear dependence of population inversion with pump

power. This may explain some experimental discrepancy in laser performance but is only a first indication since in laser or amplifier operation where high doping level are requested other phenomena may interplay with reverse cross-relaxation, like photodarkening, since pathways involve the population of Tm levels affected by reverse cross-relaxation [24-30].

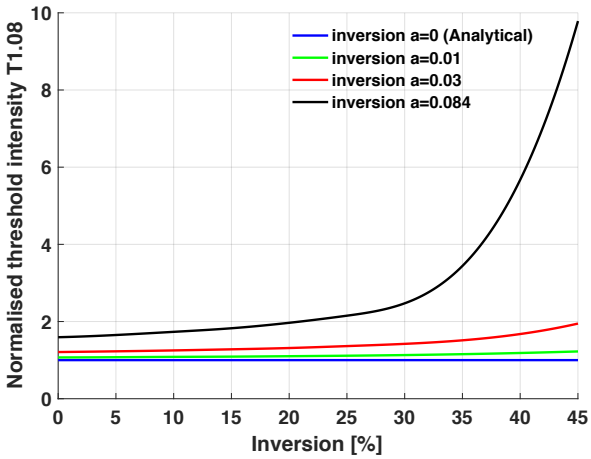

Fig. 7: Impact of reverse cross relaxation on inversion for T1.08

6. Conclusion

In this paper, we presented a comprehensive analytical model of Tm able to take into account direct cross-relaxation process. We showed that by using an appropriate set of parameters is able to properly fitting the first part of the fluorescence decay of Tm-doped tellurite glasses for different dopant concentration values. We also compared the model with a full numerical model to investigate its limitations. We assess the model is a valid tool in case of limited doping level (below 1%), or for higher doping level but with population inversion not exceeding 30%.

In this paper we presented a new analytical model, which include the cross-relaxation process. We show this model is able to properly fit the first part of Tm fluoresce decay curve and is suitable for spectroscopic experiments. We also investigated his limitation due to neglecting the reverse cross-relaxation process and we demonstrated that in case of limited doping level (below 1%) is still suitable for predicting population inversion. This model can be used to further investigate the Tm doped system and better understand the role of all spectroscopic parameter. In addition the availability of an analytic model can help to investigate the intensity noise process in Tm-doped laser by rate-equation system linearization [19].

We also plan to use the analytic model to evaluate the impact of Tm impurity on Photodarkeing process in Yb-doped glass materials [31-33].

Funding

This article is based upon work from H2020 COST Action MP1401 on "Fiber Lasers and Their Applications" supported by COST "(European Cooperation in Science and Technology)".

Reference

[1] D. Hanna, I. Jauncey, R. Percival, I. Perry, R. Smart, Electronics Letters, 24 (1988), p. 1222.
[2] S.D. Jackson, A. Lauto, Lasers in surgery and Medicine, 30 (2002), pp. 184-190.
[3] J. Allain, M. Monerie, H. Poignant, Electronics Letters, 25 (1989), pp. 1660-1662.
[4] K. Scholle, S. Lamrini, P. Koopmann, P. Fuhrberg, 2 µm laser sources and their possible applications, Frontiers in Guided Wave Optics and Optoelectronics, InTech2010.
[5] J.T. Dobler, M. Braun, J. Nagel, V.L. Temyanko, T.S. Zaccheo, F.W. Harrison, E.V. Browell, S.A. Kooi, Applications of fiber lasers for remote sensing of atmospheric greenhouse gases, Proc. SPIE2013, pp. 86011Q-86011.
[6] M. Taher, H. Gebavi, S. Taccheo, D. Milanese, R. Balda, Optics Express, 19 (2011), pp. 26269-26274.
[7] A. Godard, Comptes Rendus Physique, 8 (2007), pp. 1100-1128.
[8] A. Jha, S. Shen, M. Naftaly, Physical Review B, 62 (2000), p. 6215.
[9] T. Yamamoto, Y. Miyajima, T. Komukai, Electronics letters, 30 (1994), pp. 220-221.
[10] Q. Huang, Q. Wang, J. Chang, X. Zhang, Z. Liu, G. Yu, Laser Physics, 20 (2010), pp. 865-870.
[11] B. Richards, Y. Tsang, D. Binks, J. Lousteau, A. Jha, Optics Letters, 33 (2008), pp. 402-404.
[12] P. Peterka, B. Faure, W. Blanc, M. Karasek, B. Dussardier, Optical and Quantum Electronics, 36 (2004), pp. 201-212.
[13] S.D. Jackson, T.A. King, Journal of Lightwave Technology, 17 (1999), p. 948.
[14] C.A. Evans, Z. Ikonic, B. Richards, P. Harrison, A. Jha, Lightwave Technology, Journal of, 27 (2009), pp. 4026-4032.
[15] H. Gebavi, D. Milanese, R. Balda, S. Taccheo, J. Fernandez, J. Lousteau, M. Ferraris, Journal of Luminescence, 132 (2012), pp. 270-276.
[16] D.A. Simpson, G.W. Baxter, S.F. Collins, W. Gibbs, W. Blanc, B. Dussardier, G. Monnom, Journal of non-crystalline solids, 352 (2006), pp. 136-141.
[17] H. Gebavi, D. Milanese, G. Liao, Q. Chen, M. Ferraris, M. Ivanda, O. Gamulin, S. Taccheo, Journal of non-crystalline solids, 355 (2009), pp. 548-555.
[18] A. Albalawi, S. Varas, A. Chiasera, H. Gebavi, W. Albalawi, W. Blanc, R. Balda, A. Lukowiak, M. Ferrari, S. Taccheo, Optical Materials Express, 7 (2017), pp. 3760-3768.
[19] S. Taccheo, P. Laporta, O. Svelto, G. De Geronimo, Applied Physics B: Lasers and Optics, 66 (1998), pp. 19-26.
[20] K. Ennser, G. Della Valle, M. Ibsen, J. Shmulovich, S. Taccheo, IEEE photonics technology letters, 17 (2005), pp. 1468-1470.
[21] B.M. Walsh, N.P. Barnes, M. Petros, J. Yu, U.N. Singh, Journal of Applied Physics, 95 (2004), pp. 3255-3271.
[22] D. McCumber, Physical Review, 136 (1964), pp. A954-A957.
[23] D.A. Simpson, G.W. Baxter, S.F. Collins, W. Gibbs, W. Blanc, B. Dussardier, G. Monnom, Journal of non-crystalline solids, 352 (2006), pp. 136-141.
[24] S. Taccheo, H. Gebavi, A. Monteville, O. Le Goffic, D. Landais, D. Mechin, D. Tregoat, B. Cadier, T. Robin, D. Milanese, Optics Express, 19 (2011), pp. 19340-19345.
[25] S. Jetschke, S. Unger, A. Schwuchow, M. Leich, J. Fiebrandt, M. Jäger, J. Kirchhof, Optics Express, 21 (2013), pp. 7590-7598.
[26] M. Broer, D. Krol, D. DiGiovanni, Optics letters, 18 (1993), pp. 799-801.
[27] C. Millar, S.R. Mallinson, B. Ainslie, S. Craig, Electronics Letters, 24 (1988), pp. 590-591.
[28] J.-F. Lupi, M. Vermillac, W. Blanc, F. Mady, M. Benabdesselam, B. Dussardier, D.R. Neuville, Optics Letters, 41 (2016), pp. 2771-2774.
[29] R. Piccoli, T. Robin, T. Brand, U. Klotzbach, S. Taccheo, Optics express, 22 (2014), pp. 7638-7643.
[30] H. Gebavi, S. Taccheo, D. Milanese, A. Monteville, O. Le Goffic, D. Landais, D. Mechin, D. Tregoat, B. Cadier, T. Robin, Optics express, 19 (2011), pp. 25077-25083.
[31] S. Jetschke, M. Leich, S. Unger, A. Schwuchow, J. Kirchhof, Optics express, 19 (2011), pp. 14473-14478.
[32] H. Gebavi, S. Taccheo, L. Lablonde, B. Cadier, T. Robin, D. Méchin, D. Tregoat, Optics letters, 38 (2013), pp. 196-198.
[33] H. Gebavi, S. Taccheo, D. Tregoat, A. Monteville, T. Robin, Optical Materials Express, 2 (2012), pp. 1286-1291.
[34] S. Taccheo, private communication.